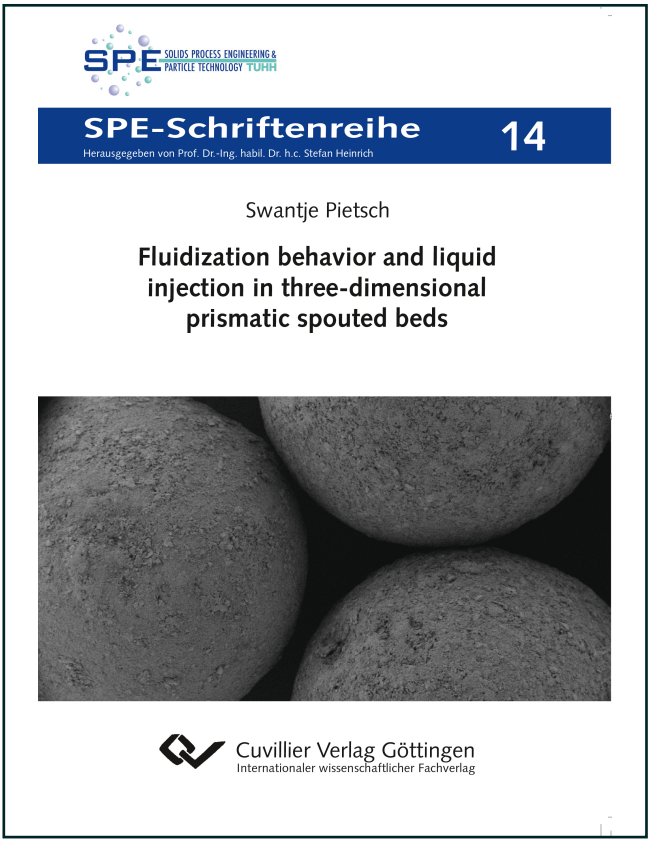

1

Introduction

1.1 Spouted bed technology

Particles, which are difficult to handle in fluidized beds due to their size or surface properties, can be fluidized in spouted beds. The term *spouted bed* has been introduced by Mathur and Gishler in 1954 (Ernest and Mathur, 1957) to describe a type of dense-phase solids operation by which they could dry moist wheat particles which had caused slugging during fluidized bed operation. The spouting can be obtained with a gas or a liquid, whereby the fluidization quality with a liquid is reported as low (Mathur and Epstein, 1974). Therefore, spouting is mostly investigated with gas media and the research of this thesis is focused on the gas-solid process.

1.1.1 General process description

In contrast to fluidized beds the gas enters the process chamber via a slit or a narrow circular inlet instead of a distributor plate over the whole cross-sectional area. The smaller cross-section of the gas inlet causes high gas velocities that accelerate particles, which gives the typical spout pattern. Due to the increasing cross-sectional area with height and the decreasing gas velocity, the upward particle transport is decelerated and the particles fall from the mushroom-shaped fountain zone at the highest point of the spout along the apparatus walls back into the ground area, which is called annulus zone. From these zones with dense particle packing, the particles move again into the gas inlet area and the circulation cycle repeats. The flow pattern is more directed and less random than in fluidized beds as shown in figure 1.1, which results in improved heat, mass and momentum transfer. Because of the high gas velocities in the spout region and the resulting vigorous particle circulation, higher temperatures than in analogous

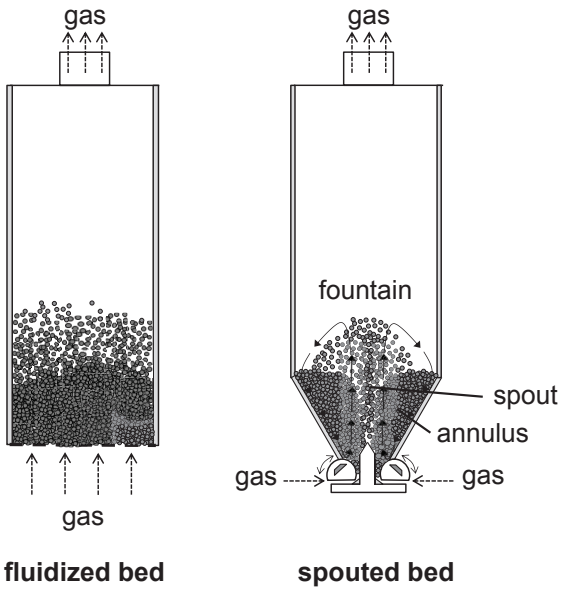

FIGURE 1.1: Comparison of flow patterns in a fluidized (left) and a spouted bed (right) apparatus.

fluidized bed operation can be used and the risk of single spots with high temperatures is reduced (Epstein and Grace, 2011). This is advantageous for drying purposes as well as for processing of temperature-sensitive material as e.g. enzymes, which usually must not exceed temperatures higher than 60 °C in order to avoid denaturing (Toole and Toole, 2008).

Since its invention different types of spouted beds have been developed, which are categorized as axisymmetric, asymmetric or slot-rectangular. The three-dimensional apparatus investigated in this thesis can be assigned to the category of slot-rectangular spouted beds and is often termed as prismatic. The apparatus geometry has been investigated intensively by Gryczka (2009) and Salikov (2017) in a pseudo two-dimensional variant in order to reduce the computational effort. The gas inlet in the present prismatic apparatus is realized by two parallel slits whose heights are adjustable by two rotatable, flattened cylinders (Mörl et al., 2001). By temporary decreasing the slit height, the gas velocity is increased which allows loosening of blockages without a stopping of the process. Besides the geometry of the apparatus, the flow pattern in a spouted bed and its stability depend on the gas velocity, the particle bed height and the properties of the bed and wall material. For a given geometry and particle type, a regime map can be obtained indicating the different spout regimes and their transitions. The spout regime is then dependent on the gas velocity: At low gas velocities, the particle bed remains static, which is termed as the fixed bed region. With increasing gas velocity, bubbles are

formed that ascend to the bed surface. The regime of stable spouting is reached at the so-called minimum spouting velocity (u_{ms}). Here, the typical spouted bed flow pattern with its three zones, namely spout, fountain and annulus zone, can be observed. By further increasing the gas velocity the spout shows instabilities, which can be seen by lateral deflections and by variations in the bed expansion height. Mathur and Gishler (1955) created regime maps by plotting the bed depth against the superficial air velocity for example for Ottawa sand fluidized in a spouted bed column with a diameter of 152 mm. Salikov et al. (2015b) obtained a regime map for a pseudo two-dimensional prismatic spouted bed apparatus made of polycarbonate with 1.8 mm γ-Al2O3 particles. In their proposed dimensionless depiction the particle Reynolds number in the inlet slits is plotted against the ratio between the height of the gas inlet slit h and the static bed height H_{st}. The spouting stability was experimentally characterized and quantified by Salikov et al. (2015b) via observations with a high-speed camera and by fast Fourier transform (FFT) of pressure drop fluctuations measured with a high frequency pressure detector. Also Freitas et al. (2004), Chen et al. (2008), Piskova and Mörl (2008), Gryczka et al. (2009) and others used a Fourier transform of the bed pressure drop for analysis of the spouting stability in rectangular spouted beds. The power spectra obtained by Freitas et al. (2004) show a well-defined dominant frequency between 5 and 7.5 Hz as an attribute of the dense stable spouting in a slot-rectangular bed with a single vertical gas inlet. Gryczka et al. (2009) found a similar dominant frequency as a characteristic value of stable spouting in the prismatic spouted bed with two adjustable gas inlets (about 6 Hz). A frequency of around 6 Hz for the same prismatic apparatus was confirmed by Salikov et al. (2015b). Salikov et al. (2015b) could increase the range of stable spouting by inserting two parallel plates into the process chamber. They found that the area above the middle profile and the interface between the spout and the annulus zone are characterized by oscillations and spout deflections, which can be reduced by the plates. Luo et al. (2004) found the installation of draft plates in their investigated slot-rectangular spouted bed to result in an unstable "conveying-moving bed" after a bubbling and slugging regime. The installation of additional stabilizers in spouted beds has also been reported for other geometric types. Altzibar et al. (2008) reported a reduced fountain height and a higher drying efficiency with a conical spouted bed equipped with a draft tube. They found the minimum spouting velocity, the peak pressure drop and the operating pressure drop to be influenced by the geometric factors of the tube (Altzibar et al., 2009).

At high gas velocities, Salikov et al. (2015b) ascertained a second stable spouting regime with lower particle void fractions, namely the dilute or jet spouting, which had not been reported before. They recommended the dilute spouting regime for low to intermediate bed masses in large apparatuses due to the increased risk of particle elutriation and

defined it promising for the stable spouting of very fine particles. Brandt et al. (2013) and Wolff et al. (2014) made use of the dilute spouting in a prismatic process chamber with a very large free-board zone for the granulation of µm-sized ceramic particles with a thermoplastic polymer in order to produce homogeneous composites with ultrahigh packing density. Similarly, Eichner et al. (2017) conducted spray coating in the dilute spouting regime of a specially designed prismatic apparatus with a large relaxation zone to achieve uniformly polymer coated µm-sized copper particles.

In fluidized beds the bed pressure drop increases linearly with the gas velocity during the fixed bed state until the minimum fluidization velocity u_{mf} is reached and fluidization is initialized. During fluidization of the bed, the pressure drop is constant and independent of the gas velocity. In case of a spouted bed, the pressure drop-gas velocity behavior is different. Again, the bed pressure drop is linearly increasing but after that a bed pressure drop peak occurs which is caused by first bubbles bursting the bed surface. Afterwards the bed pressure drop is drastically decreasing to a point at which spouting begins (u_{ms}). During stable spouting the bed pressure drop is almost constant but decreases when reaching the instable spouting regime.

Geldart (1973) classified particles according to their properties and the resulting fluidization behavior into four different classes from A to D. Group A particles have a particle size between 20 and 100 µm and a density below 1400 $\mathrm{kg\,m^{-3}}$. Beds consisting of this material expand considerably before bubbling occurs. Geldart group B includes particles in a size range between 40 and 500 µm with a density between 400 and 1400 $\mathrm{kg\,m^{-3}}$ and shows bubbling at the minimum fluidization velocity. Group C particles are small and cohesive powders with a particle size between 20 and 30 µm and are difficult to fluidize. Particles categorized into group D are large and/or dense particle powders which require high gas volume flow rates for fluidization. In this thesis, microcrystalline cellulose particles and alumina (γ-Al2O3) particles were investigated, both in a particle diameter range of around 500 µm with densities of about 1300 $\mathrm{kg\,m^{-3}}$ and thereby classified as Geldart B particles. For the alumina particles, additional studies were performed with particles of 1.8 mm and 3.0 mm size.

In contrast to fluidized beds no universal equations for the calculation of the maximum bed pressure drop or the minimum spouting velocity exist but a lot of correlations for different geometries are available, which differ in the particle range or bed geometry that they are valid for or in the properties that they take into account. Due to their quite broad range of bed geometries and particle properties the correlations by Olazar et al. (1992) for conical and cylindrical columns, respectively, are recommended for the estimation of the maximum pressure drop if the pressure drop at stable spouting is known [16]. For slot-rectangular spouted beds e.g. Rocha et al. (1995) and Mitev (1979)

obtained correlations for the maximum bed pressure drop, where the column diameters in the equation of Rocha et al. (1995) are the equivalent diameters calculated from the rectangular area of the process chamber. The more general correlation of Mitev (1979) contains an empirical correction factor J, which depends on the geometry of the apparatus and the properties of the particle bed:

$$\begin{aligned} \Delta p &= J g \rho_\mathrm{s} H_\mathrm{st} (1 - \varepsilon_\mathrm{mf}) \\ \text{with} \quad J &= 1.2 \quad \text{for} \quad H_\mathrm{st} < 180 \text{ mm} \quad \text{and} \\ J &= 0.72 \cdot 10^{1.26 \cdot H_\mathrm{st}} \quad \text{for} \quad H_\mathrm{st} > 180 \text{ mm}, \end{aligned} \tag{1.1}$$

with the gravitational constant g and the porosity ε. For fluidized beds this correction factor is equal to 1. The minimum spouting velocity for cone-base cylindrical columns with a diameter smaller than 0.5 m is usually calculated by the equation obtained by Mathur and Gishler (1955):

$$u_\mathrm{ms,cyl} = \frac{d_\mathrm{p}}{d_\mathrm{col}} \left(\frac{d_\mathrm{col,in}}{d_\mathrm{col}} \right)^{\frac{1}{3}} \sqrt{\frac{2gH(\rho_\mathrm{s} - \rho_\mathrm{f})}{\rho_\mathrm{f}}}, \tag{1.2}$$

where d_p is the particle diameter, d_col is the diameter of the column, $d_\mathrm{col,in}$ is the inner diameter of the column, H is the bed height and ρ_f the density of the fluid. For the dimensions of the investigated prismatic *ProCell* apparatuses and the used particle sizes, no correlation for the calculation of the minimum spouting velocity is known in literature. In addition, most of the known correlations for conical and cylindrical vessels were developed for column diameters of 61 cm or even smaller with reported problems in fitting the experimental results for higher diameters (Mathur and Epstein, 1974).

Since its original invention for drying purposes, spouted bed technology has been adapted for a wide field of applications. Most of them include an additional phase, namely a liquid phase, for agglomeration, granulation or spray coating (see figure 1.2). During agglomeration several core particles are connected by a liquid binder, whereas in spray granulation particle growth is obtained by solidification of liquid droplets around single core particles. The principle of spray coating is similar to granulation but much smaller layer thicknesses are desired. Particle coating is widely used in various industries, as e.g. for food, detergents and fertilizer processing or in pharmaceutical applications. The main challenge is the formation of a homogeneous layer without cracks and voids in order to protect the core material from the environment or to protect the environment from an unwanted release of the core material. Often, the coating is applied on active substances like pharmaceutical ingredients or enzymes, which should be released under and only under defined conditions as a certain pH value in the gastro-intestinal system or on agricultural fields. Besides the homogeneous distribution on the scale of one single

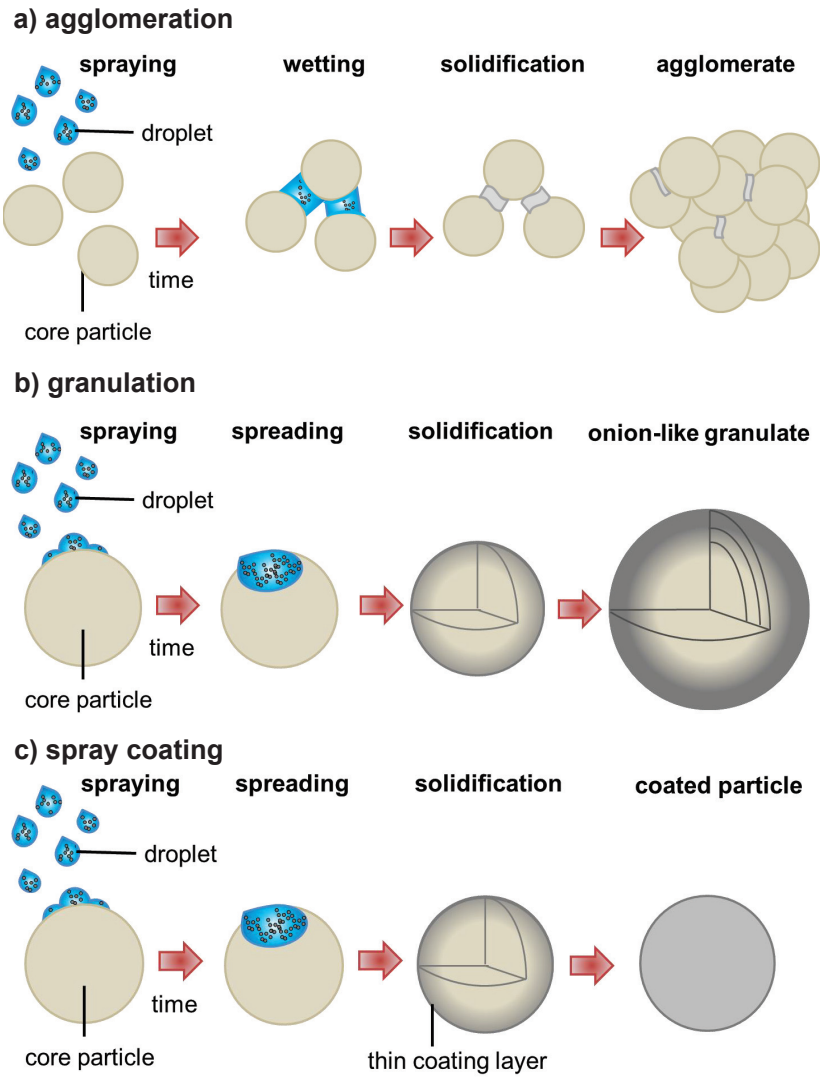

FIGURE 1.2: Principle of particle growth due to a) agglomeration, b) granulation and c) spray coating.

particle, the homogeneous coating of the entire particle bed in one production charge is a criterion of quality. Due to the high importance of the coating quality for product value, its measurement has been investigated with different tools within the last years. The methods can be differentiated into in-line, on-line, at-line and off-line procedures, whereby the in-line measurement is preferred as it allows a fast investigation without an interruption of the process (Knop and Kleinebudde, 2013). Classical measurement techniques are based on an external, non-real-time analysis: A representative sample is

taken from the process at given time points and measured externally by e.g. electron microscopy or particle size analysis or by analysis of the time-dependent dissolution behavior. For example van Kampen et al. (2015) analyzed the coating quality of sodium chloride particles coated with maltodextrin in a fluidized bed process by measuring the dissolution rate of the core material. Klukkert et al. (2016) applied multispectral UV imaging to measure the tablet film coating quality of tablets produced in a pan coater. They could detect cracks on the surface and differentiate between homogeneous and inhomogeneous coatings. In general, the sampling has the disadvantage of a process disturbance due to the interception of particles by a sampling device. Additionally, human labor is needed and the analyzed particles have to be discarded, which increases waste and decreases process efficiency. Different in-line measurement techniques, as e.g. Raman or near-infrared (NIR) spectroscopy and their application in the field of particle technology have been described in literature within the last years. Romero-Torres et al. (2006) used Raman spectroscopy to quantify the coating layer thickness during pan coating of tablets with methylcellulose, polyethylene glycol and a blue fluorescent dye. By application of partial least squares calibration algorithm they were able to measure the layer thickness in an interval between 50 to 151 µm, which refers to the range of a linear relationship between the fluorescent layer thickness and the Raman spectral data. For measurement of smaller layer thicknesses a more detailed calibration work would be necessary as proposed by the authors. Recently, Barimani and Kleinebudde (2018) used Raman spectroscopy to measure the end points in coating processes with colored tablets. They used six differently colored coatings with pigments and/or dyes, whereby again some of them caused fluorescence and thereby interfering with the Raman signal. Similar to the work of Romero-Torres et al. (2006) different calibration methods were tested, whereby the partial least square algorithm led to the best model performance parameters. This algorithm was able to predict the endpoints of all coating experiments until a total coating time of 50 min, which was related to coating thicknesses between 21 and 38 µm. Lee et al. (2011) investigated a fluidized bed process for coating of pharmaceutical pellets, where they measured the layer thickness with NIR spectroscopy. They used external methods, namely confocal laser scanning microscopy (CLSM) and laser diffraction particle size analysis (LD-PSA), for the NIR calibration model. Layer thicknesses between 0 and 90 µm were detected. Even though deviations of CLSM and LD-PSA measurements occurred in the interval between 30 and 60 µm, both calibration models were found to have correlations with R^2 values exceeding 0.995. When an appropriate number of spectra was taken for averaging, the accuracy of the thickness prediction of NIR with the calibration models was greater than 99 %. Gendre et al. (2011) showed that real-time NIR measurements can be performed on non-finished drug products to predict the dissolution properties of the cured coated tablets, which is important in terms of quality criteria of sustained release coated particles. The study

was performed with three different calibration models. Cahyadi et al. (2010) compared different non-destructive methods, X-ray fluorescence (XRF) as well as Raman and NIR spectroscopy, to quantify the thickness of tablet (6 µm size) coatings. For model calibration they used data from cut cross-section analysis with stereomicroscope. XRF was shown to be a useful method to quantify the amount of coating applied onto the tablet but errors in thickness measurements occurred. Both NIR and Raman spectroscopy were able to predict the non-linearity of coating thickness but only Raman was found to be capable of differentiating tablets coated under different conditions. May et al. (2011) introduced the terahertz pulsed imaging (MPI) measurement as a non-intrusive in-line measurement technique for coating thickness determination. By means of a waveform processing and analysis algorithm in Matlab, the data stream from the coating sensor was analyzed in real-time. The results from in-line measurements agreed well with off-line MPI data and with weight gain measurements. Nevertheless, the measurement time was with 9 min for one single particle time consuming and direct measurements of coating thickness were only possible with a minimum layer thickness of 40 µm. Recently, the application of optical coherence tomography (OCT) for coating layer measurement has been introduced. The method has been widely used for medical imaging but also other application fields were reported before (Stifter, 2007). For example the tomography method was used as quality control tool for paper characterization (Fabritius et al., 2006), silicon integrated circuits (Serrels et al., 2010) or fiber composites (Stifter et al., 2008). For tracking coating processes, it has been first introduced by Koller et al. (2011). Since then, the method has been successfully applied to coating processes in fluidized beds (Markl et al., 2015b), pan coaters (Markl et al., 2015a, 2014) or drum spray coaters (Markl et al., 2014). Optical coherence tomography is an interferometric approach, which makes use of the coherence properties of light in order to obtain depth profiles of investigated semi-transparent and turbid materials in a contactless and non-destructive way (Fercher, 2010, Wojtkowski, 2010). The generated cross-section images are obtained by measuring the magnitude and the time delay of light, which is reflected back from the sample. By using core particles and coating suspensions with different refractive indices, the layer thickness is accessible. It is also possible to characterize multilayer structures, whereby a minimum thickness of 10 µm is necessary as this is the resolution limitation. The algorithm in the work of Koller et al. (2011) has been implemented in the in-line OCT measurement unit used by Markl et al. (2015a,b). The system was kindly borrowed by this research group of Prof. Khinast from the Research Center Pharmaceutical Engineering (Graz, Austria) for experimental investigations on the applicability of the method for the regarded laboratory spouted bed.

1.1.2 Continuous operation

As all gas-solid processes, spouted beds can be performed in batch or continuous operation, whereby throughputs between 20 $\mathrm{kg\,h^{-1}}$ and 10000 $\mathrm{kg\,h^{-1}}$ are common (Glatt Ingenieurtechnik GmbH, 2006). In batch operation, the material is fed into the chamber before the process is started and is collected after the process has been stopped. Batch processes are mainly used for research, whereas in industry continuous operation with high productivity is preferred for efficiency. Continuous spouted beds are often of prismatic geometry configuration, whereby the scale-up from smaller scale is performed by increasing the depth of the apparatus. Pilot scale plants often consist of several stages, which are serially connected. With this configuration, different unit operations as e.g. granulation, coating and drying can be realized afterwards in one process. The series connection of unit operations in one plant requires a certain residence time of the particles in every single stage to ensure that for example the coating layer is of required thickness or drying is sufficient. Additionally, back-mixing has to be avoided as e.g. already coated particles should not return into the granulation zone but enter the drying area. In order to measure and adjust the movement of particles through continuous gas-solid processes, the knowledge of their residence time distribution (RTD) is of great importance. The residence time is defined as the time that a particle needs to get from the inlet of the apparatus to its outlet. For a general description of residence time behavior, ideal and real reactors are distinguished (Levenspiel, 1999). In case of ideal reactors, two defined border cases exist, the ideal stirred tank reactor and the ideal plug flow reactor (see figure 1.3). In ideal stirred tank reactors, a perfect micro-mixing is assumed resulting in a homogeneous concentration independent of the location in the apparatus at every time. In continuous operation, every particle has the same residence time in the reactor. Ideal plug flow reactors are based on the continuous flow of a flat profile, which results in concentrations that are depending on the location but independent of the time. Again, every particle needs the same time from inlet to outlet.

The behavior of particles in real reactors deviates from perfect micro-mixing and from perfect velocity profiles, which is caused by different flow velocities of fluids, dead zones and bypasses. As a consequence thereof, particles need different times to pass the process chamber. For quantification of the residence time behavior, exit age distributions are used. It is assumed that the flow is stationary and incompressible ($\rho_\mathrm{f} = \mathrm{const.}$), the transport at the in- and outlet is caused by forced convection and that the boundary condition closed-closed according to Danckwerts (1953) is valid. This condition means that a particle, which has entered the plant, is not able to leave it through the inlet again and that a particle that has left the reactor through the outlet cannot enter it again. For mathematical description of residence time behavior, the fraction of particles

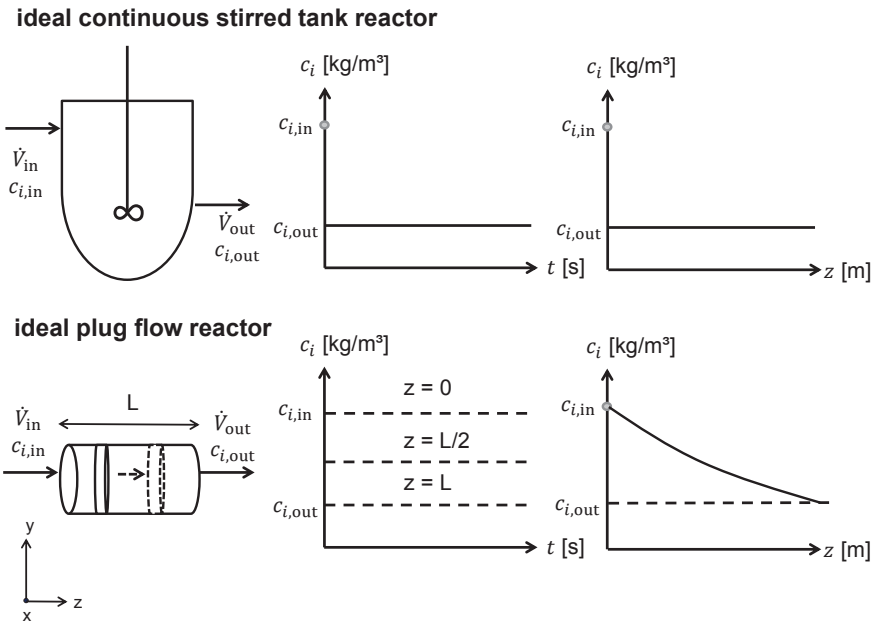

FIGURE 1.3: Time- and location-dependent concentration profiles of ideal reactors; top: ideal continuous stirred tank reactor (CSTR), bottom: ideal plug flow reactor.

leaving the reactor in time interval Δt is plotted against the time t, which results in the exit age distribution $E(t)$ with the unit s^{-1}. The dimensionless value $F(t)$, defined as $F(t) = \int_0^t E(t)\,dt$, gives the fraction of particles with a residence time less than t in the reactor, whereby after an infinitely long period all particles have left the apparatus:

$$F(t) = \int_0^t E(t)\,dt, \tag{1.3}$$

$$\int_0^{t_i} E(t)\,dt < 1; \qquad \int_0^{\infty} E(t)\,dt = 1. \tag{1.4}$$

The first moment μ_1 of the exit age distribution gives the mean residence time $\bar{t}$ of particles in the reactor:

$$\mu_1 = \bar{t} = \int_0^{\infty} t^1 E(t)\,dt. \tag{1.5}$$

If the density does not change and no dead volumes or bypasses occur, the mean residence time is equal to the hydrodynamic residence time τ that is calculated from the reactor volume V_R and the particle volume flow rate $\dot{V}_p$:

$$\tau = \frac{V_R}{\dot{V}_p}. \tag{1.6}$$